1

AMIDR: A Complete Pulse Method for Measuring Cathode Solid-State Diffusivity

Mitchell Ball[1], Marc Cormier[2], Eniko Zsoldos[1], Ines Haman[2], Svena Yu[3], Ning Zhang[2], Nutthaphon Phattharasupakun[2,4], Michel B. Johnson[2], Michael Metzger[1,2], Chongyin Yang[1,2], and Jeff Dahn[1,2,z]

[1] Department of Chemistry, Dalhousie University, Halifax, Nova Scotia B3H 4R2, Canada

[2] Department of Physics and Atmospheric Science, Dalhousie University, Halifax, Nova Scotia B3H 4R2, Canada

[3] Department of Process Engineering and Applied Science, Dalhousie University, Halifax, Nova Scotia B3H 3J5, Canada

[4] Department of Chemical and Biomolecular Engineering, School of Energy Science and Engineering, Vidyasirimedhi Institute of Science and Technology, Rayong 21210, Thailand

[z] Corresponding author – Jeff.Dahn@dal.ca

1

Abstract

The Atlung Method for Intercalant Diffusion and Resistance (AMIDR) is a novel, high accuracy method for measuring solid state diffusivity and interface resistance related to the Atlung Method for Intercalant Diffusion (AMID) with several key differences. Most notably, AMIDR is designed to analyze the voltage response over time of "complete" pulses, pulses that last until an impedance steady state is reached. These differences allow for AMIDR to return diffusivity results with a higher degree of confidence than Galvanostatic Intermittent Titration Technique (GITT) and at a faster rate with higher state of charge (SOC) resolution than Electrochemical Impedance Spectroscopy (EIS). In this study, three different lithium transition metal oxides were studied. These active materials showed very similar kinetic behaviour that varied with dependence on the fraction of Ni atoms filling sites in the Li layer. AMIDR comes with a user-friendly python program complete with a user interface that is intended to assist other researchers in measuring active material diffusivity in a controlled, repeatable manner. This program, along with instruction on its use, the results of this study from raw data to the final key kinetic metrics, and a video summary of AMIDR design are available for download at https://github.com/MitchBall/AMIDR.

2

Introduction

When a current is applied to a Li-ion cell, lithium ions are transported from the electrolyte to the surface of an active material or vice versa at a certain flux. Transport within the active material from the surface to the interior and vice versa relies on solid-state diffusion. This diffusion is driven by lithium concentration gradients transporting lithium from high concentration locations to low concentration locations in the active material. Diffusion shrinks these concentration gradients over time encouraging uniform concentration throughout an active material particle. However, when a current is applied, transport between the active material and the electrolyte also occurs and concentration changes at the particle surface encourage non-uniformity. As solid-state diffusion is not often infinitely fast compared to the surface flux, this can lead to significantly low or high concentrations at the active material particle surface compared to the interior. The potential of an electrode particle is dependent upon the concentration of lithium at its surface, and therefore poor diffusion can lead to undesirably high or low potentials during charge or discharge, respectively. This change in potential from an ideal case where solid-state transport is infinitely fast is often regarded as an overpotential. This overpotential, as well as overpotential from resistance, is a source of lost energy. Diffusion overpotential stores energy in the concentration gradient of the active material which is later expelled as heat when diffusion occurs, whereas resistance overpotential is just simply expelled as heat immediately. Additionally, these overpotentials may cause the cell voltage limit to be reached prematurely, effectively limiting the capacity of an active material. It is essential that cell voltage limits are not surpassed as potentials that are too high or low can cause degradation at the surface of the active material even though the interior is at a more stable potential.

52   Solid-state diffusion occurs at both electrodes in most Li-ion or similar cells with the

53   exception being lithium metal cells where lithium is deposited on the surface of a lithium metal

54   electrode and does need to be transported further. This study focuses on accurately measuring the

55   lithium diffusivity in lithium nickel manganese cobalt (NMC) layered oxide cathode active

56   materials which are commonly spherically shaped and have kinetically hindered capacities.

57   However, the methods used here may be applied to other active materials, both cathode and

58   anode, and even other transport ions such as Na^+ or K^+, with appropriate modification.

59   **Theory**

60   *Impact of Geometry on Diffusion Transport*

61   Particle shape is important to consider when measuring impedance from diffusion. A

62   change in concentration is first created at the surface and this encourages changes in

63   concentration further within the active material as time goes on. Figure 1 shows common

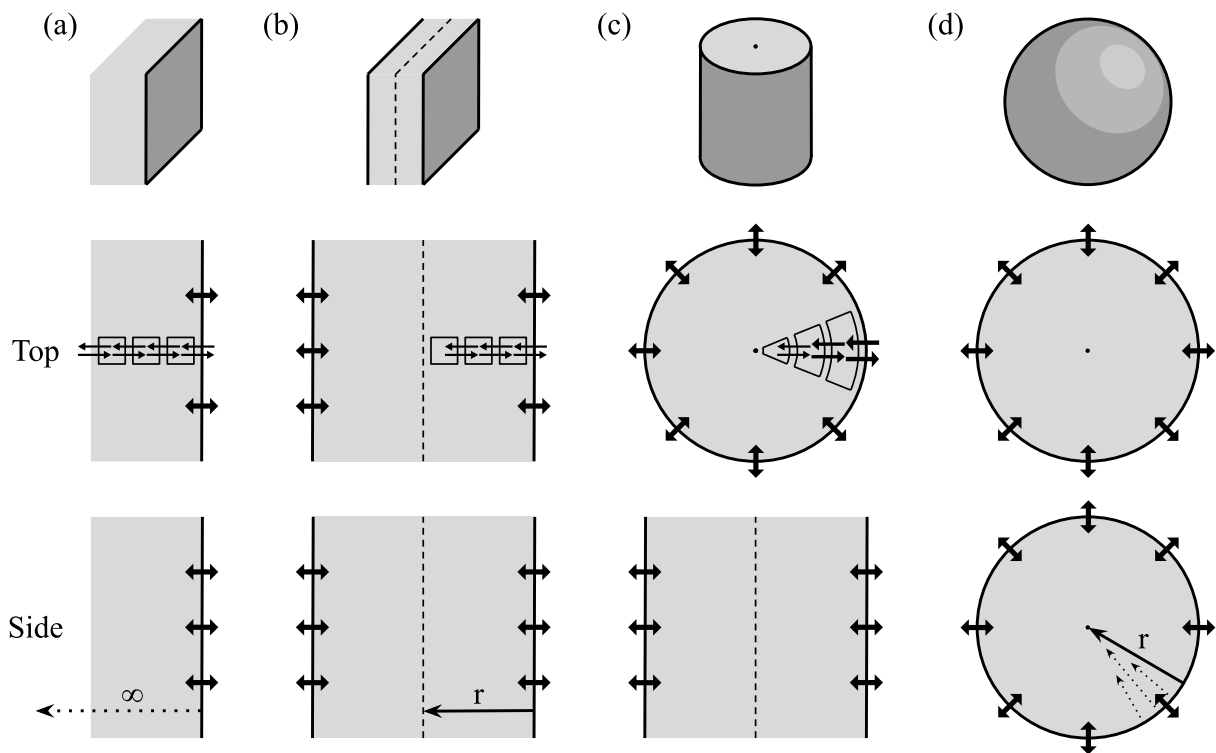64   geometries for modeling diffusion.

4

Figure 1: Simplified geometries for modeling diffusion. The given geometries are (a) semi-infinite plane, (b) planar sheet, (c) cylinder, and (d) sphere.

The simplest model is the semi-infinite plane (Figure 1a), a volume that is infinite in all directions except the surface in contact with electrolyte. This is the easiest geometry to model, but in practice, diffusion cannot continue infinitely. Ions transported from the electrolyte will eventually arrive at a position furthest into the interior of the active material and transport cannot occur further beyond this position. The distance from the electrolyte contacting surface to the furthest interior position is the diffusion length or radius (cm), r, for circular geometries. The planar sheet (Figure 1b) is similar to the semi-infinite plane but instead has two electrolyte contacting surfaces and a central plane forming the furthest interior position. The planar sheet can also be used to model a volume with one electrolyte contacting surface and one non-contacting surface by splitting the geometry in half along the central plane. When ions eventually

5

78   stop at the end of r, this slows diffusion transport along the diffusion path which causes a greater

79   change in concentration at the electrolyte contacting surface compared to a semi-infinite plane.

80   The shape of the active material may cause ions to transport inwards from a larger

81   volume to a smaller volume or vice versa. This is the case for the cylindrical and spherical

82   models (Figure 1c-d) which have some radial rather than linear geometry. This will also

83   similarly slow diffusion transport and cause a greater change in concentration at the surface than

84   in a planar sheet or an ideal semi-infinite plane.[1]

85   In practice, all active materials have finite volumes. While only the sphere is truly finite,

86   all geometries can be used to approximate more complex finite geometries. The planar sheet and

87   sphere mark the maximum and minimum bounds for the volume to surface area ratio (cm), $\tilde{V}/S$,

88   of all geometries with a fixed r. As a result, the planar sheet and sphere also mark the maximum

89   and minimum bounds of diffusion hindrance for geometries with a fixed r.

90   *Surface Concentration due to Diffusion Transport*

91   The interplay between transport at the active material surface induced by an applied

92   current and transport within the active material determines the surface concentration.

93   Conveniently, it has been shown that all real morphologies will approximate a semi-infinite

94   plane at the start of a constant flux or constant current (CC) pulse applied to a "relaxed" active

95   material, active material starting with a uniform concentration. This is because the start of a

96   pulse only meaningfully changes concentrations within a very thin layer near the surface which

97   can easily be approximated as a semi-infinite plane. The solution to the change in surface

98   concentration (mol cm^{-3}), Δc_s, of semi-infinite plane experiencing a CC pulse starting from a

99   uniform concentration has been proven to be

6

100
$$\Delta c_s(t) = \frac{2J\sqrt{\Delta t}}{\sqrt{\pi D_c}},$$
(1)

101 where $J = Iz^{-1}F^{-1}S^{-1}$ is the ionic flux (mol s^{-1} cm^{-2}), Δt is the period (s) of pulse time, and D_c

102 is chemical diffusivity (cm^2 s^{-1}), the material property of interest when determining the speed of

103 ion diffusion.[2] I is the current (A) being applied, z is the ion charge number (+1 for lithium), F is

104 Faraday's Constant (C mol^{-1}), and S is the surface area (cm^2) exposed to electrolyte. This

105 equation is likely familiar to anyone with experience using the Galvanostatic Intermittent

106 Titration Technique (GITT). It can be helpful to normalize this equation into dimensionless

107 variables which produces

108
$$X_s(\tau) = \frac{2\sqrt{\tau}}{A\sqrt{\pi Q}},$$
(2)

109 where $X_s = \Delta c_s / \Delta c_{tot}$ is the relative change in surface concentration, $\tau = \Delta q / \Delta q_{tot}$ is the

110 relative change in capacity, $Q = \Delta q_{tot} I^{-1} D_c r^{-2}$ is the relative diffusivity, a normalized measure

111 of how fast diffusion transport is compared to the surface flux, and A is a geometric constant

112 sourced from the inverse $\tilde{V}/S$ for certain geometries (1 for a planar sheet, 2 for a cylinder, 3 for a

113 sphere). $\Delta c_{tot} = n_{tot}/\tilde{V}$ is the change in concentration if an arbitrary, desired n_{tot} number of

114 moles (mol) of ions are transported and uniformly dispersed in a volume (cm^3), $\tilde{V}$, of an active

115 material. $\Delta q_{tot} = zFn_{tot}$ is the arbitrary capacity (C) associated with n_{tot}, and $\Delta q = zFn = I\Delta t$

116 is the actual capacity acquired after a certain Δt where n moles are transported. τ can also be

117 treated as relative moles transported or relative pulse time given that Δq is proportional to n and

118 Δt when I is constant. One of the advantages of using dimensionless convention is that it

7

119   normalizes the variables and describes pulses of all I and active materials of all D_c and r

120   simultaneously as long as the active material geometry is the same.

121   After the start of a pulse, modelling X_s gets more complicated. The numerical solution for

122   X_s of active material during a pulse starting from a relaxed state has been shown to be

123
$$X_s(\tau) = \tau + \frac{1}{AQ}\left(\frac{1}{B} - 2\sum_{i=1}^{\infty}\frac{e^{-\alpha_i^2 Q\tau}}{\alpha_i^2}\right),$$
(3)

124   where the ascending, non-zero series α_i is defined for each geometry as

125   Planar Sheet: $\sin(\alpha) = 0 \{\alpha_1 = \pi, \alpha_2 = 2\pi, \dots\}$,

126   Cylinder: $J_1(\alpha) = 0$,

127   Sphere: $\alpha\cot(\alpha) - 1 = 0$,

128   B is another geometric constant (3 for a planar sheet, 4 for a cylinder, 5 for a sphere), and J_1 is

129   the Bessel function of the first kind of order 1. This dimensionless convention and the complete

130   equation for describing X_s resulting from diffusion transport was developed by Atlung, the

131   namesake of AMID and AMIDR.[1] It's unfortunate that the solution to equation 3 must be

132   numerical rather than analytical, but it is at least far simpler than more opaque numerical

133   solutions from techniques such as the Finite Element Method (FEM).

134   Despite being numerical, equation 3 will often approximate analytical solutions.

135     $\lim_{Q\to\infty^+} X_s(\tau) = \tau$, showing that if D_c is infinitely fast, the concentration, c, in the active material

136   is uniform and c_s has a linear relationship with Δq. This scenario is ideal as this means that no

137   energy will be lost, and the active material can be considered impedance-free. While not

8

138 obvious, it has been shown that $\lim_{\tau \to 0^+} X_s(\tau)$ is equation 2, proving that all geometries approximate

139 a semi-infinite plane at pulse start.[2] In addition,

$$\lim_{\tau \to \infty^+} X_s(\tau) = \tau + \frac{1}{ABQ}. \qquad (4)$$

141 This shows that as Δq approaches Δq_{tot}, the active material eventually reaches a steady state

142 where X_s approaches a linear relationship with τ, and c_s approaches a linear relationship with

143 Δq. Once this steady state is reached, the pulse can be described as a "complete" pulse that has

144 reached its "end". Using this terminology, a pulse that has been stopped before a steady state has

145 been reached is said to have been stopped before it has reached its end.

146 Figure 2 shows that the simple analytical equations 2 and 4 form the lower and upper

147 bounds for the otherwise more complex numerical equation 3. While the sphere has the most

148 diffusion limitation from shrinking volumes along the diffusion path and most quickly deviates

149 from equation 2, it is the ideal geometry for minimizing X_s deviation from the impedance-free

150 scenario due to its decreased $\tilde{V}/S$. The difference between $Q = 0.5$ (Figure 2a) and $Q = 2$

151 (Figure 2b) shows that larger Q is more desirable to limit X_s deviation from the impedance-free

152 scenario. Lastly, Figures 2a and b have the same shape, but different size. These two graphs

153 could be describing the same pulses, just with a different n_{tot} desired moles of ions to be
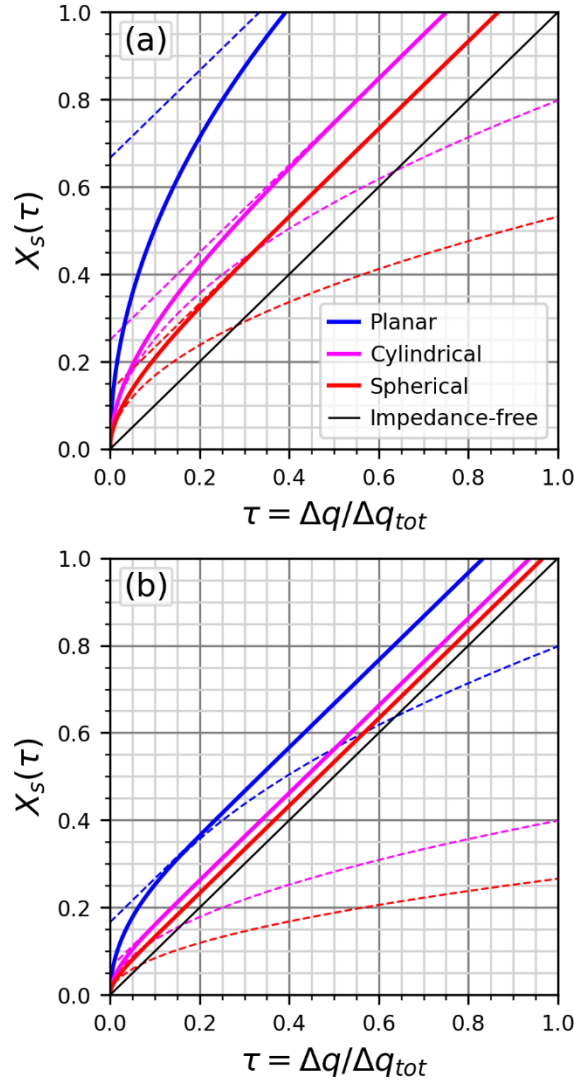
154 transported.

9

Figure 2: The relationships between relative change in capacity, τ, and relative change in surface concentration, X_s, of planar, cylindrical, and spherical active material during a short pulse when relative diffusivity, (a) $Q = 0.5$ and (b) $Q = 2$. These relationships are compared to the ideal, impedance-free relationship when $Q \to \infty^+$. The inverse quadratic and linear dashed lines, where visible, represent the lower and upper limits for X_s as τ approaches 0 and ∞^+.

Capacity Limitation due to Diffusion Transport

Poor diffusion can cause the Δc_s to reach a certain limit defined by a voltage limit stopping a pulse before significant utilization of the interior of the active material. This is because the potential of the active material is determined by c_s. This limit can be defined as

10

165   when $\Delta c_s = \Delta c_{tot}$ and in dimensionless convention, defined as when $X_s(\tau) = 1$. Inserting this

166   into equation 3 gives

$$1 = \tau + \frac{1}{AQ}\left(\frac{1}{B} - 2\sum_{i=1}^{\infty}\frac{e^{-\alpha_i^2 Q\tau}}{\alpha_i^2}\right), \tag{5}$$

168   which gives a relationship between Q and τ for when this limit is reached. In the same manner as

169   equations 2 and 4, this relationship can be given the bounds

$$1 = \frac{2\sqrt{\tau}}{A\sqrt{\pi Q}}, \text{ and} \tag{6}$$

$$1 = \tau + \frac{1}{ABQ}. \tag{7}$$

172   Figure 3 shows this relationship and its bounds. When Q is significantly small, the

173   relationship approaches equation 6 for when τ is small and the limit is reached near the start of

174   the pulse before a steady state is approached. This is undesirable as a small τ means far less than

175   the desired n_{tot} moles of ions were transported. Alternatively, when Q is significantly large, the

176   relationship approaches equation 7 for when τ is large and the limit is reached near the end of the

177   pulse when the active material has reached a steady state. In this case, nearly all the desired n_{tot}

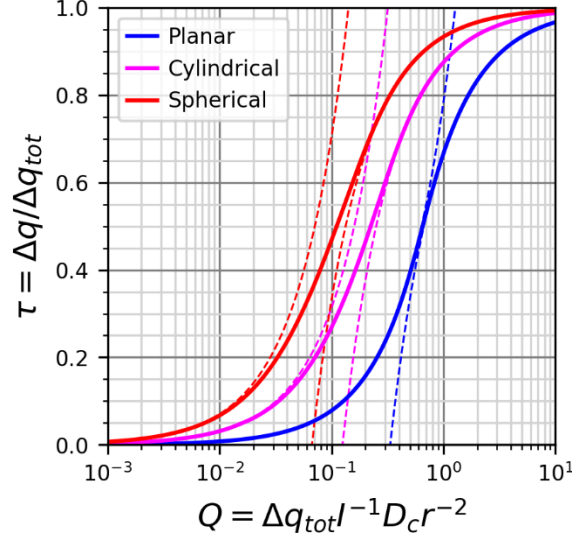178   moles of ions are transported.

179

Figure 3: The relationship between relative diffusivity, Q, and relative change in capacity, τ, of planar sheet, cylindrical, and spherical active materials when a relative surface concentration limit is reached, $X_s = 1$, and a pulse is stopped. The exponential dashed lines represent the upper and lower limits for τ as τ approaches 0 and ∞^+.

Impedance due to Diffusion Transport

In an ideal, impedance-free scenario, the concentration throughout the active material is uniform and the ideal X_s, $X_{s,ideal}$, increases from 0 to 1 equivalently with τ as shown in Figure 2 ($X_{s,ideal} = \tau$). The difference between X_s and $X_{s,ideal}$ can be defined as $X_{s,loss} = X_s - X_{s,ideal}$. $X_{s,loss}$ can also be calculated by simply subtracting τ from equation 3 to get

$$X_{s,loss}(\tau) = \frac{1}{AQ}\left(\frac{1}{B} - 2\sum_{i=1}^{\infty}\frac{e^{-\alpha_i^2 Q\tau}}{\alpha_i^2}\right). \tag{8}$$

Next, this can be converted out of dimension-less convention to get

$$\Delta c_{s,loss}(\Delta t) = \frac{Ir^2}{AzF\tilde{V}D_c}\left(\frac{1}{B} - 2\sum_{i=1}^{\infty}\frac{e^{-\alpha_i^2\frac{\Delta t D_c}{r^2}}}{\alpha_i^2}\right). \tag{9}$$

12

192   where $\Delta c_{s,loss}$ is the non-relative difference in surface concentration from an ideal impedance-

193   free scenario. The surface concentration, c_s, of an active material determines its potential (V), E,

194   so $\Delta c_{s,loss}$ implies a difference in E from an ideal, impedance free scenario. The relationship

195   between c_s and E for any active material is complex but can be simplified to a simple linear

196   relationship (V cm^3 mol^{-1}), dE/dc, if the E range is small enough. Accordingly, $c_{s,loss}$ can be

197   converted into a diffusion overpotential (V), η_D, for a working electrode as

$$\eta_D(\Delta t) = -\frac{dE}{dc}\frac{Ir^2}{AzF\tilde{V}D_c}\left(\frac{1}{B} - 2\sum_{i=1}^{\infty}\frac{e^{-\alpha_i^2\frac{\Delta t D_c}{r^2}}}{\alpha_i^2}\right). \tag{10}$$

199   where positive I is now treated as current driving positive ions to leave the active material, the

200   typical convention for working electrodes. dE/dc is not a commonly used metric in cell analysis

201   but differential capacity (C/V), dq/dV is. $q = zF\tilde{V}(c_{sat} - c)$ is the capacity of charge stored in

202   the active material of the working electrode where c_{sat} is the fully saturated concentration

203   corresponding to no charge being stored. $V = E_w - E_c$ is the total voltage (V) of a cell where E_w

204   is the potential of the working electrode and E_c is the potential of the counter electrode. This

205   study uses a half cell arrangement where the counter electrode is lithium metal and will treat

206     $E_c = 0\ V\ vs.Li^+/Li^0$. Therefore $dq/dV = -zF\tilde{V}dc/dE$. With this, equation 10 can be further

207   simplified to

$$\eta_D(\Delta t) = \frac{Ir^2}{AD_c\frac{dq}{dV}}\left(\frac{1}{B} - 2\sum_{i=1}^{\infty}\frac{e^{-\alpha_i^2\frac{\Delta t D_c}{r^2}}}{\alpha_i^2}\right). \tag{11}$$

13

209   The relationship between Δt and η_D retains the same shape as the relationship between τ and X_s

210   shown in Figure 2. Conveniently, related to equation 4, after a long period of time, equation 11

211   can be simplified to

212
$$\lim_{\Delta t \to \infty^+} \eta_D(\Delta t) = \frac{Ir^2}{ABD_c \frac{dq}{dV}}. \tag{12}$$

213   Even more conveniently, this can be further simplified as

214
$$R_{D,term} = \frac{r^2}{ABD_c \frac{dq}{dV}}, \tag{13}$$

215   where $R_{D,term}$ is the terminal diffusive resistance (Ω) given that $V = IR$. This is particularly

216   powerful as this means that the impedance related to diffusion can be approximated as a simple

217   resistance given a long enough period of time. This has a very practical application as it can be

218   used to predict voltage polarization for long, CC charges/discharges or the maximum voltage

219   polarization for intermittent pulses.

220   *Combining Diffusion Impedance and Resistance*

221   Diffusion is not the only source of impedance in a cell. Impedance can come from a

222   variety of sources from electrical resistance in the current collectors and the conductive additive

223   to ionic impedance in the electrolyte, both in and outside of the electrode pores, and reaction

224   impedance at the electrode-electrolyte interfaces. In addition, many of these impedance sources

225   are paired with capacitances such as double layer capacitance at the electrode-electrolyte

226   interfaces, and parallel plate capacitance across the two electrodes within coin cells. The

227   impedance of the opposing electrode can be ignored if using a reference electrode and the

14

228   electrolyte impedance inside electrode pores can be mitigated by using thin electrode coatings.

229   Thin electrodes amplify active material impedances by reducing the total amount of active

230   material, similar to how thin wires produce more resistance. These impedances are diffusion

231   impedance, which is dynamic on long timescales (> 1 s), and interface resistance, R_i, which is

232   effectively instantaneous on long timescales. Remaining sources of impedance are mostly

233   negligible resistances, R_{ohm}, electrical contact resistance and ionic electrolyte resistance, which

234   are also effectively instantaneous on long timescales. Also included is ionic electrolyte diffusion

235   impedance which can be dynamic over long timescales with significantly thick separators, but is

236   effectively instantaneous with standard, commercial thin separators.[3] Therefore, these can simply

237   be treated as a single resistance, $R = R_i + R_{ohm}$, producing a resistive overpotential, $\eta_R = IR$.

238   In practice, η_R can limit Δq further than η_D alone by allowing a voltage limit to be

239   reached earlier than when $X_s(\tau) = 1$. In this case, the limit can be said to be reached when

240   relative change in voltage, $Y(\tau) = 1$. $Y(\tau) = (\Delta V_i(\Delta t) + \eta_D(\Delta t) + \eta_R)/\Delta V_{tot}$, where $\Delta V_i(\Delta t) =$

241    $\Delta q (dq/dV)^{-1}$ is the ideal, impedance-free change in voltage after a certain period of pulse time,

242   and $\Delta V_{tot} = \Delta q_{tot}(dq/dV)^{-1}$ is the total change in voltage from the initial voltage to the voltage

243   limit. Evaluating this equation returns

$$Y(\tau) = \tau + \frac{1}{AQ}\left(\frac{1}{B} - 2\sum_{i=1}^{\infty}\frac{e^{-\alpha_i^2 Q\tau}}{\alpha_i^2}\right) + \frac{IR(dq/dV)}{\Delta q_{tot}}. \tag{14}$$

245   This equation is very similar to equation 3 except for the inclusion of a new term at the end. This

246   new term can be converted into dimensionless units as

$$Y(\tau) = \tau + \frac{1}{AQ}\left(\frac{1}{B} - 2\sum_{i=1}^{\infty}\frac{e^{-\alpha_i^2 Q\tau}}{\alpha_i^2}\right) + \frac{P}{Q}, \tag{15}$$

15

248   where $P = RD_c r^{-2}(dq/dV)$ is the relative resistance, a variable comparing η_R to η_D, similar to a

249   Biot number. When $P \ll 1/AB$, Δq is primarily limited by η_D, and the last term can be neglected

250   to simplify the entire equation back to equation 3. However, when $P \gg 1/AB$, the last term is

251   large, and Δq is primarily limited by η_R rather than η_D. Setting $Y(\tau) = 1$ gives the relationship

252   between Q and τ for when a voltage limit is reached,

253
$$1 = \tau + \frac{1}{AQ}\left(\frac{1}{B} - 2\sum_{i=1}^{\infty}\frac{e^{-\alpha_i^2 Q\tau}}{\alpha_i^2}\right) + \frac{P}{Q}, \tag{16}$$

254   similar to equation 5 except with the addition of the last term.

255   Figure 4a shows the relationship posed by equation 15 and Figure 4b shows the

256   relationship posed by equation 16. Increasing P increases η_R and reduces the proportion of τ

257   capable of being transported before a voltage limit is reached. Additionally, Figure 4b shows that

258   increasing P changes the relationship between Q and τ from a pseudo-logistic shape to a pseudo-

259   exponential shape. While the shape of the curve changes significantly with small τ, the shape of

260   the curve remains the same at large τ. This is because η_D approximates η_R when τ is large and

261   the difference between η_D and η_R become indistinguishable without information from earlier in
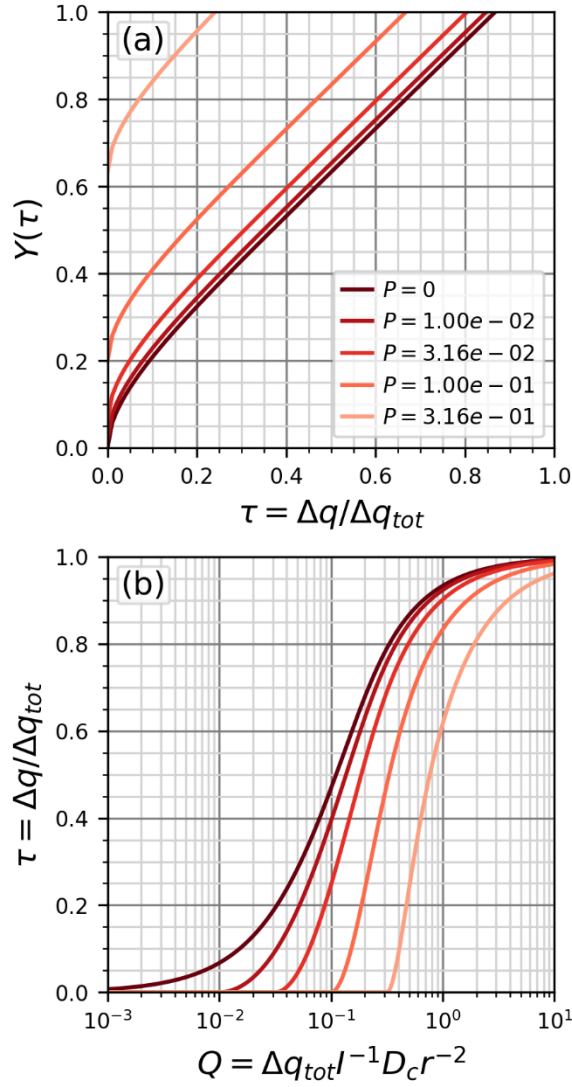
262   the pulse.

Figure 4: The relationship (a) between relative change in capacity, τ, and relative change in voltage, Y, of a cell during a short pulse when relative diffusivity, $Q = 1$ and the relationship (b) between τ and Q, when a voltage limit is reached, $Y = 1$. The active material is given a spherical geometry and relative resistance, P, is varied to show the impact of resistance.

Impact of Diffusion Length Variation due to a Particle Size Distribution

The mathematical model for impedance resulting from diffusion is designed for a single geometry but can easily be scaled up for an ensemble of geometries of identical r keeping in mind that I, q, n, and $\tilde{V}$ should represent the total values for the entire ensemble. However, in practice, geometries such as active material particles often have a measurable variation in r. This presents a problem because ensembles of geometries with varying r do not experience constant

17

274   flux throughout a pulse which is essential for this model. While flux is equal for all geometries at

275   the start of a pulse, flux at the end of the pulse is proportional to the $\tilde{V}/S$ of a geometry because

276   the I of each geometry is proportional to its q and therefore $\tilde{V}$. This means larger particles

277   increase in flux and smaller geometries decrease in flux throughout the pulse. Despite not being

278   able to develop a complete, simple mathematical model for the impedance of a pulse upon active

279   material with a distribution in r, the bounds for pulses that stop near their start and end with

280   active material of varying r can be calculated. These bounds are simply the original equations 6

281   and 7 with different average r values, $\bar{r}$, as inputs. These $\bar{r}$ are calculated as $\bar{r}_s = \sum r_j^3 / \sum r_j^2$ and

282    $\bar{r}_e = \left(\sum r_j^5 / \sum r_j^3\right)^{1/2}$ for the start and end of a pulse respectively, where r_j is r for an individual

283   geometry (see Proofs S1 and S2). Figure 5 shows the impact of a theoretical bimodal active

284   material on the relationship between Q and τ. The theoretical bimodal active material used in this

285   model is composed of spheres of r equal to 1 arb. units and 3 arb. units in a 1:1 q ratio. The r

286   used to calculate Q for this bimodal active material is calculated as the capacity-weighted

287   geometric mean as $\bar{r} = 10^{\frac{\sum \log r_j * r_j^3}{\sum r_j^3}}$. The multiplicative change in Q between the uniform and

288   bimodal model can be regarded as a Q-shift calculated as $(\bar{r}_s/\bar{r})^2$ or $(\bar{r}_e/\bar{r})^2$. While the complete

289   model for bimodal active material cannot be plotted, it is clear that it would not differ from a

290   uniform r active material by a dramatic amount. All active materials analyzed in this study have

291   less particle size variation than this theoretical model, so while particle size variation may add

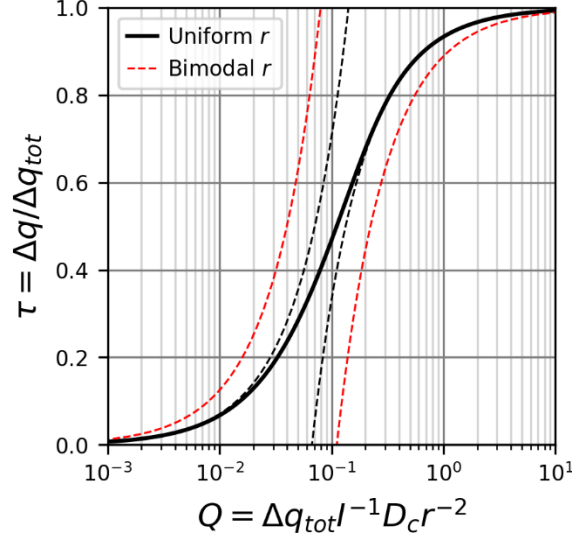292   some error to the model, the model is still reasonably accurate (see Table S1).

18

Figure 5: The relationship between relative diffusivity, Q, and relative change in capacity, τ, for uniform and bimodal spherical active materials when a surface concentration limit is reached, $X_s = 1$, and a pulse is stopped. The bimodal active material is composed of spheres of radius 1 arb. units and 3 arb. units in a 1:1 capacity ratio. The diffusion length, r, for the bimodal active material is calculated as the capacity-weighted geometric mean. The dashed lines represent the upper and lower limits for τ as τ approaches 0 and ∞^+.

Interface Contact Resistivity

While not all resistance in a cell is sourced from the electrode-electrolyte interface, an overwhelming portion can be, especially in cells designed with little active material mass loading. If it is believed that the overwhelming majority of measured R is R_i, then that R_i can be normalized as contact resistivity (Ω cm^2), $\rho_c = R_i S$. This describes the resistivity of current traveling through a film of unknown or infinitesimally thin thickness and is separate from bulk resistivity (Ω cm), which describes the resistivity of current traveling through a bulk material, and sheet resistance (Ω), which describes the resistivity of current traveling along a film of unknown thickness.[4] In the context of active material, ρ_c is calculated as

$$\rho_c = SR = \frac{ARm}{r\rho_d}, \tag{17}$$

19

310   where m is the mass (g) of the active material and ρ_d is the density (g cm^3) of the active

311   material.

312   *Chemical Diffusivity vs. Tracer Diffusivity*

313   While it is common in literature to report lithium diffusion in Li-ion cells as simply "Li

314   diffusivity" there is more than one kind of D measurement and differentiating between them can

315   be valuable for understanding the mechanisms of diffusion. If an isotope of a solute is used as a

316   tracer to track random particle movement in a uniform concentration, tracer diffusivity, D_t is

317   measured. This is different from chemical diffusivity, D_c, which is measured by observing the

318   transport of a solute from a high concentration to a low concentration. These two are the same in

319   dilute concentrations where all solutes have the same atomic environment and diffusion from a

320   high to a low concentration is driven solely by solute particles independently moving at random.

321   However, in concentrated solutions, D_t stays the same, but D_c changes due to solute-solute

322   interactions not present in dilute concentrations. These solute-solute interactions cause solutes to

323   have the different enthalpies at different concentrations and this difference in enthalpy can drive

324   or hinder diffusion from high to low concentrations.

325   The relation between chemical potential (J mol^{-1}), μ, and c is known to be

326 $$\mu(c) = \mu_0 + N_A k_B T ln(\gamma(c)c), \tag{18}$$

327   where μ_0 is the intrinsic chemical potential (J mol^{-1}), N_A is the Avogadro constant (mol^{-1}), k_B is

328   the Boltzmann constant (J K^{-1}), T is temperature (K), and γ is the activity coefficient. In dilute

329   solutions, γ is constant. In concentrated solutions, solute-solute interactions occur, γ is not

330   constant and the relationship between μ and c is complex. Active materials often have a complex

331   relationship between μ and c because ions are typically stored in solids as concentrated solutions.

332   This is easily observed in q-V plots of active materials which typically do not show a logarithmic

333   relationship. The solute-solute interactions in active materials often present themselves as

334   changes in occupation site enthalpies due to structural distortions at different c.[5] The relationship

335   between D_t and D_c is described by Darken's second equation for a single phase medium,

336
$$D_c(c) = D_t(c)\left(1 + \frac{dln(\gamma(c))}{dln(c)}\right),$$
(19)

337   where $D_t = D_c$ when γ is constant at dilute concentrations.[6] This can be converted into an

338   equation with more practical variables. Taking the derivative of equation 18 in terms of c gives

339
$$\frac{d\mu}{dc} = \frac{N_A k_B T}{c}\left(1 + \frac{dln(\gamma(c))}{dln(c)}\right),$$
(20)

340   which share the conversion term given in Darken's second equation. Given this, equation 19 can

341   be simplified to

342
$$D_c(c) = D_t(c)\frac{c}{k_B T}\frac{d\mu}{dc},$$
(21)

343   and given that $d\mu = -zFdV$, $zFV_m c = (q_{sat} - q)$, and $F = q_e N_A$, where q_{sat} is the theoretical

344   capacity capable of being stored given complete saturation and desaturation and q_e is the

345   elementary charge (C), it can be made to use dq/dV as

346
$$D_c(q) = D_t(q)\frac{zq_e(q_{sat} - q)}{k_B T \frac{dq}{dV}}.$$
(22)

21

347   While D_c is the relevant diffusivity measurement for describing ion transport in the active

348   material of a cell under operation, D_t has a relatively simple derivation modeled by a random

349   walk,

350
$$D_t = \frac{a^2 \left(1 - \frac{c}{c_{sat}}\right) v}{2C} e^{-\frac{\Delta G_A}{k_B T}},$$
(23)

351   where a is the distance between two occupation sites (cm), c_{sat} is the concentration of a

352   completely saturated active material (mol cm^{-3}), v is the vibrational frequency (s^{-1}), C is the

353   dimensionality constant (2 for a layered oxide where ions are able to transport in 2 dimensions),

354   and ΔG_A is the activation energy (J) of an occupation site hop.[6] The $1 - c/c_{sat}$ term is included

355   to account for the chance that an occupation site hop is blocked by the destination occupation site

356   being already occupied. This term is equivalent to q/q_{sat}. It can be valuable to remove this term

357   to form a new measurement of diffusivity, D_t^*, free-path tracer diffusivity,

358
$$D_t^* = \frac{a^2 v}{2C} e^{-\frac{\Delta G_A}{k_B T}},$$
(24)

359   which describes diffusion transport for a solute with a uniform c and no occupation sites blocked

360   along its path of travel. This measurement is rather abstract but can be calculated and has

361   powerful implications. The only value in its derivation that is expected to change significantly

362   for an active material at different states of charge is ΔG_A. In this manner, D_t^* can be used as a

363   proxy to measure changes in ΔG_A at different states of charge. If D_t^* stays relatively the same at

364   varying states of charge this suggest that ΔG_A is unchanged, but if D_t^* shrinks significantly, this

365   suggests that ΔG_A has increased significantly. The relationship between D_c and D_t^* is

22

$$366 \qquad D_c(q) = D_t^*(q) \frac{zq_eq\left(1 - \frac{q}{q_{sat}}\right)}{k_BT\frac{dq}{dV}}. \qquad (25)$$

367 Lastly $R_{D,term}$ can be calculated in terms of site hopping using equations 13, 22, and 23

368 returning

$$369 \qquad R_{D,term} = \frac{2Ck_BTe^{\frac{\Delta G_A}{k_BT}}r^2}{ABzq_eq\left(1 - \frac{q}{q_{sat}}\right)a^2v}. \qquad (26)$$

370 **Prior Methods**

371 *Galvanostatic Intermittent Titration Technique (GITT)*

372 GITT is a common single-rate pulse method for measuring D_c. This method is relatively

373 easy to use because the active material is modeled as a semi-infinite plane allowing for the

374 voltage response analysis to be based on equation 1 which is a relatively simple analytical

375 solution. However, active materials of various morphologies only approximate a semi-infinite

376 plane at the very start of a pulse when transport only occurs at the very surface of the particle, so

377 GITT requires the inequality $\Delta t \ll r^2/D_c$ to be true for the approximation to be accurate.

378 Because this inequality relies on D_c, the value whose accuracy is being tested, this inequality

379 must be passed by a very large margin to not suffer from the inequality circularly proving itself.

380 For instance, it has been shown for spherical particles that if $\Delta tD_c/r^2 \approx 0.3$, the measured D_c

381 value will be underestimated by a factor of 10.[2] Because a user would use the D_c value calculated

382 by GITT to check the inequality, the inequality would be calculated as $\Delta tD_c/r^2 = 0.03$ which an

383 inexperienced user might consider as acceptable.

23

384   While this may make it tempting to perform GITT with the shortest pulses possible, this

385   can also be problematic as other sources of impedance and capacitive effects are dynamic and

386   relevant on short timescales. Therefore, accurate GITT measurements must be performed within

387   a certain window of Δt that is not always easy for the user to predict and is very unlikely to be

388   the same at all states of charge of the cell. Additionally, it is possible that under certain

389   conditions, such as when D_c is particularly high or r is particularly small, this window is shrunk

390   out of existence and there is no available Δt that will produce an accurate result.[2]

391   *Electrochemical Impedance Spectroscopy (EIS)*

392   EIS is a common alternating current (AC) method for measuring D_c. A sinusoidal change

393   in voltage (potentiostatic EIS) or current (galvanostatic EIS) at various frequencies is applied to a

394   cell and the alternating current or voltage response is analyzed respectively. The response at

395   various frequencies is calculated into real and imaginary impedance values and can be made to

396   fit various circuit models that include some or all of the various sources of impedance and

397   capacitance. The sources of impedance and capacitance that are dynamic on short timescales

398   impact the response at high frequencies and diffusion, which is typically relevant on long

399   timescales, impacts the response at low frequencies. Because all elements are being fit

400   simultaneously, EIS does not have the same trouble measuring D_c as GITT does when D_c and

401   other impedance sources are relevant at similar timescales.

402   Diffusion is very often modeled with a semi-infinite plane as the typical frequencies used

403   are not low enough for the concentration beyond the particle surface to be altered meaningfully.

404   While it has been shown that with significantly low enough frequencies, the impact of active

405   material geometry on impedance can be measured and accurately modeled, this isn't common as

406 low frequencies take longer periods of time to be measured.[7] In addition, very low frequencies

407 suffer from amplified error that must be carefully managed. This error may be introduced by

408 trying to measure very low currents for potentiostatic EIS, applying currents for very long

409 periods of time adjusting the SOC for galvanostatic EIS, or cell aging for either.

410 Acquiring D_c measurements at a high resolution versus SOC can also be challenging.

411 Between each measurement, a pulse and a significantly long rest must first be applied to adjust

412 the SOC and allow the cell to relax. Each EIS measurement may also take a significant amount

413 of time if lower frequency measurements are desired. For instance, a single 1 mHz measurement

414 consisting of 10 periods will take greater than 2 hours. This means that measuring a single cell

415 may take an infeasible amount of time considering the availability of EIS capable instruments.

416 Since multiple EIS measurements already require pulses for transitioning SOC, significant time

417 could be saved by using a method that utilizes these pulses as the source of the measurement data

418 using simpler, non-EIS capable instruments.

419 *Atlung Method for Intercalant Diffusion (AMID)*

420 AMID is a multi-rate pulse method for measuring D_c developed in this lab. As shown in

421 Figure 6, AMID is done by performing a series of pulses and rests at progressively slower

422 currents all with the same voltage limit. The starting voltage of the first pulse and the voltage

423 limit define the voltage interval of a single D_c measurement. After a single measurement, the

424 process is repeated for a new voltage interval. As the last pulse in an interval has a very small

425 current that produces very little overpotential, the starting voltage of a first pulse is very similar

426 to the voltage limit of the previous interval. The voltage interval is used to define the Δc_{tot} for X_s

427 and total change in capacity of the interval is used to estimate Δq_{tot} for τ. The change in capacity

25

428   from the end of each pulse compared to the start of the interval is used to define the cumulative

429   change in capacity, Δq_c, of each pulse. Δq_c is approximated as Δq for τ when $X_s = 1$. Given the

430   selection of spherical geometry, a r value measured with SEM images, and the I value

431   corresponding to each pulse, the data is fit to equation 5 using D_c and Δq_{tot} as fitting parameters

432   with the error in τ being minimized (Δq_{tot} is a fitting parameter because the total change in

433   capacity for the interval will be somewhat less than Δq_{tot}). The D_c value acquired is recorded as

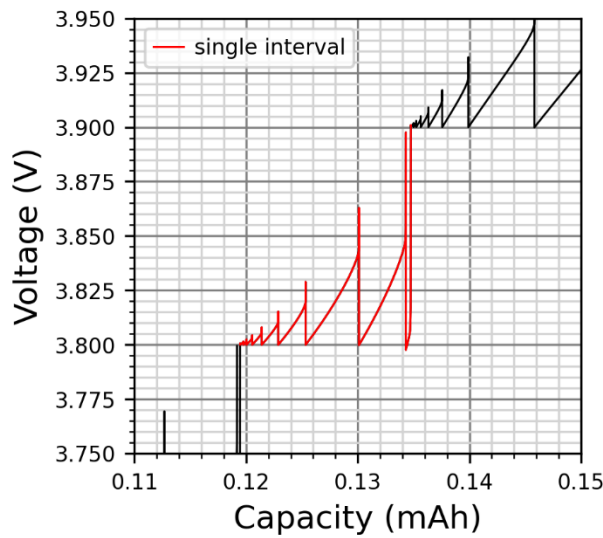434   representative for that interval.

435

436   Figure 6: Example of a portion of an AMID protocol in discharge. A single interval composed of
437   descending pulses and ascending rests is highlighted in red.

438   The approximation of Δq_c as Δq has been shown to be a reasonable approximation for

439   low current pulses that don't result in a small τ.[8] This is because η_D becomes constant and

440   approximates an η_R at the end of a pulse when τ is large. Once η_D has reached a steady state, it

441   does not matter when the pulse started. η_D will be the same and, therefore, the Δq_c acquired at

442   the voltage limit will be the same as Δq. AMID limits the influence of high I pulses with

443   dynamic η_D by weighting each pulse by the sum of the η_R of all other pulses in an interval.

444   Unfortunately, pulses with dynamic η_D are important for differentiating η_D from η_R. AMID cells

26

445   are designed to mitigate other sources of impedance through cell build by selecting low

446   impedance electrolyte and low mass loading electrodes to remove electrolyte impedance within

447   the electrode pores and amplify η_D. Unfortunately, reducing electrode mass loading also

448   amplifies R_i by the same proportional amount. This means that AMID will have a systemic error

449   for all active materials with a high R_i. Additionally, the voltage intervals for AMID are typically

450   rather large (0.1 V or greater) limiting the SOC resolution.

451   **Atlung Method for Intercalant Diffusion and Resistance (AMIDR)**

452   AMIDR is a new method for measuring D_c similar to AMID but with a series of

453   modifications such as the use of a GITT-style, single-rate, iterating pulse and rest protocol shown

454   in Figure 7, and a novel approach for accounting for resistance. Exact details necessary for

455   replication of this study are available in Chapter 6: Experimental, whereas design considerations

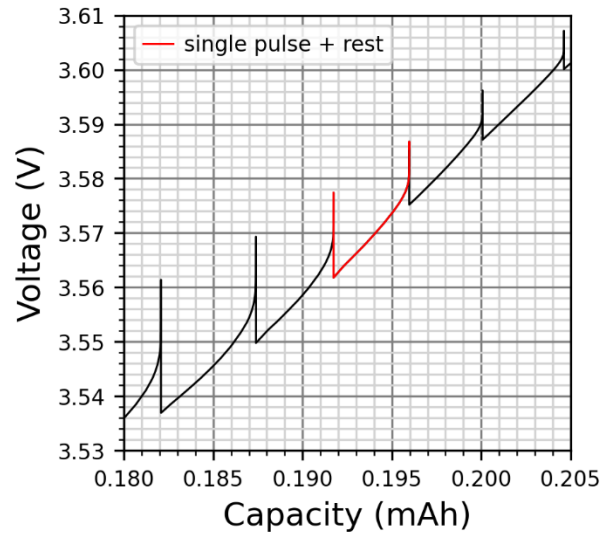456   are given within this section.

457

458   Figure 7: Example of a portion of an AMIDR protocol in discharge. A single descending pulse and
459   ascending rest is highlighted in red.

460   *Cell Design*

27

461   AMIDR cells are quite similar to AMID cells in that they have very low mass loading

462   and electrolyte selected to reduce impedance. Mass loading is reduced to the point that the

463   current collector is somewhat visible beneath the electrode coating. This ensures that there are no

464   particles layered on top of each other limiting the electrolyte impedance within the pores to be

465   negligible. In addition, it also reduces the active material mass amplifying the active material

466   impedance sources, diffusion impedance and interface resistance. These very low mass loading

467   coatings can be achieved by reducing the active material:solvent ratio and selecting a very low-

468   profile coating blade. In addition, thin separators (20 μm) are selected so that the ionic electrolyte

469   diffusion impedance can be regarded as a resistance on long timescales.

470   Different from AMID, AMIDR cells typically use a reference electrode. The reference

471   electrode allows the counter electrode impedance to be neglected which is valuable as the

472   counter electrode typically has impedance that develops on a similar timescale as the working

473   electrode impedance and, therefore, cannot be neglected as simply R. The reference electrode

474   selected is a 50 μm Au wire insulated with a 7 μm polyimide coating often referred to a micro-

475   reference electrode (μ-RE). After cutting and stripping the polyimide coating on either ends of

476   the wire to allow for electrical contact, the wire is threaded into a coin cell during the cell build

477   process (see Figure S2). Once the cell is built, the reference electrode must be lightly lithiated to

478   produce a AuLi alloy. This alloy has been shown to produce a stable ~0.31 V vs. Li^+/Li^0 which

479   allows it be used as a reference electrode.[9,10]

480   *Testing Apparatus*

481   The reference electrode has very little contact area with the electrolyte which gives it a

482   significant amount of resistance and very little double layer capacitance at its interface. This

483   means that even a small amount of induced current from ambient electromagnetic radiation will

28

484   contribute to a very large change in the measured potential. In this manner, the reference

485   electrode can act like an antenna unless properly shielded. The only way to ensure that the

486   reference electrode does not produce any induced current is to shield the entire cell and all its

487   wires up to the cell tester. This can be done with shielded cables and aluminum foil attached to a

488   ground in combination with an insulating wrapping material such as nitrile gloves to prevent

489   shorts and ground loops (see Figure S3).

490   AMIDR cannot be performed accurately on just any cell tester. The cell tester must be

491   able to apply and measure a current with reasonable accuracy ($\pm$ 1 μA), but great stability ($\pm$ 1

492   nA) within a period < 0.1 s from the start of the pulse. This is because while AMIDR will work

493   with any current small enough, that current needs to be kept stable and measurable for the

494   assumption of constant flux at the active material surface to be held true. Similarly, the cell tester

495   must be able to measure and record voltage at high frequency (< 0.1 s) and great accuracy ($\pm$ 0.1

496   mV). This voltage measurement accuracy requirement can be compensated for with even higher

497   frequency measurements by averaging voltage measurements together to produce voltage

498   measurements with less noise. These requirements have been determined for coin cells with Li

499   layered oxide active material and the requirements might need to be adjusted for different cell

500   formats and active materials. For instance, a very low mass loading pouch cell will likely not

501   require such low current accuracy and an active material with rapidly changing impedance over a

502   small change in voltage will likely require more accurate voltage measurement.

503   *Data Analysis*

504   Rather than using a multi-rate pulse protocol like AMID, AMIDR uses a single-rate pulse

505   protocol similar to GITT. This allows for a greater resolution of D_c over SOC. Additionally,

29

506   while AMIDR is still based upon the mathematics described by Atlung, modification is made to

507   account for R.

508   While it may be tempting to define ΔV_{tot} as the total change in voltage of the pulse and

509   simply fit Y over τ of a single pulse to equation 15 as shown in Figure 4a, this equation is not

510   well suited for fitting. Firstly, the initial slope of Y over τ is infinite meaning that any slight error

511   in τ due to error in current measurement or cell capacitive effects will result in a massive error in

512   Y which is an issue if the fit is produced by minimizing error in Y. Secondly, τ and Y are much

513   larger towards the end of the pulse which means that minimizing error in τ or Y will give

514   significantly more weighting to the end of the pulse.

515   Instead, ΔV_{tot} is defined as the change in voltage from the pulse start for each individual

516   data point and the total dataset is then fit to equation 16 as shown in Figure 8a and 8b. In this

517   manner, $Y(\tau) = 1$ is set for each individual data point as if each data point reached its own

518   voltage limit. For clarity's sake, it is helpful to change a few variable names. $\Delta q_{tot} =$

519    $(dq/dV)\Delta V_{tot}$ can be rewritten as $\Delta q_i = (dq/dV)\Delta V$ where Δq_i is the ideal, impedance-free

520   change in capacity corresponding to ΔV, the actual change in voltage, of every point. Q and τ are

521   now redefined as $Q = \Delta q_i I^{-1} D_c r^{-2}$ and $\tau = \Delta q/\Delta q_i$. dq/dV is calculated as $dq/dV = \Delta q_0/\Delta V_0$

522   where Δq_0 and ΔV_0 are the changes in capacity and voltage from the start of the pulse to the

523   termination of the relaxation period after the pulse. In this manner, the calculated dq/dV is free

524   from impedance and purely thermodynamically determined. Given the selection of spherical

525   geometry and Δq as the change in capacity for each point, the pulse is fit to equation 16 using Q

526   and P as fitting parameters with the error in τ being minimized. Then, given a r value measured

527   with SEM images (see Figure S1) and I for the pulse's current, R and D_c are calculated. Lastly,

30

528   ion saturation and D_t^* can optionally be calculated with the assistance of regular mass loading

529   cell data to account for poor active mass accuracy when using low mass loading cells (see Table
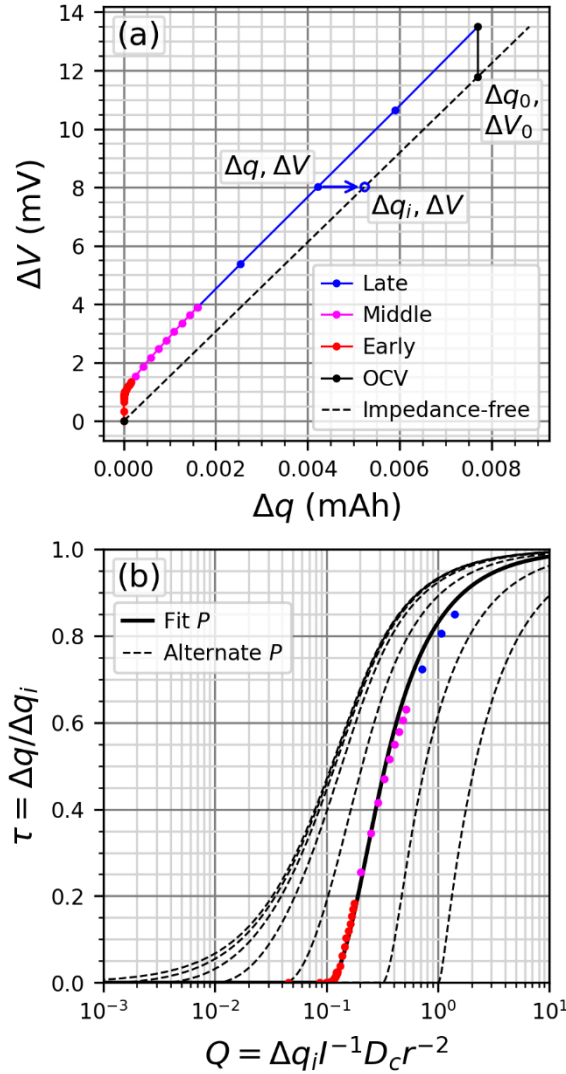
530   S3).

531

532   Figure 8: The transformation of pulse data to optimize fitting accuracy from (a) a pulse plotted with
533   widely recognizable axes of change in capacity, Δq, and change in voltage, ΔV, to (b) the same pulse
534   plotted with axes of relative diffusivity, Q, and relative capacity, τ, which is much better suited for fitting
535   because all periods of the pulse are equally weighted.

536   This method using equation 16 is much better suited for fitting as the greatest change in τ

537   over change in Q is not vertical mitigating any error in τ produced by error in Q. Additionally,

538   because error in τ is being minimized and τ is a normalized measurement of capacity, equal

31

539   weighting is given throughout the pulse. Lastly, spherical geometry is selected as most active

540   materials have a form that is more spherical than it is cylindrical or planar. Technically, layered

541   oxides might be better represented as a series of cylinders of varying r as diffusion primarily

542   occurs within the layers of the lattices. However, due to the inconsistent flux that these cylinders

543   experience due to varying r, this representation cannot be explained by the simple mathematical

544   model presented in this study. Regardless, there is relatively little difference (less than a factor of

545   3) between the values of D_c measured by fitting to a cylindrical or spherical model because there

546   is relatively little difference between the values of Q for a cylindrical and spherical model as

547   seen in Figure 3.

548   All of these steps of analysis as well as data visualization tools are combined into a user

549   friendly, python program designed to allow users with minimal programming experience to run

550   their own AMIDR experiments and rapidly analyse AMIDR test files. This program is built off

551   the AMID framework and therefore can analyze AMID test files as well. In addition, it also

552   includes a series of optional features to help with cell tester file format conversion, fitting of

553   erroneous data, and even the ability to analyse AMID datasets with AMIDR mathematics (even

554   though this is typically not recommended). Also included within the package containing this

555   program are the datasets analyzed within this study, so that a new user can practice the analysis

556   process, and an experienced impedance expert can verify the results presented here.

557   *Protocol Design*

558   AMIDR analyzes a series of single-rate discharge pulses followed by a series of single-

559   rate charge pulses after 1.5 cycles of formation (see Figure S5). This protocol is split between

560   multiple protocol instruction files due to cell tester limitations but also to allow for some

32

561   flexibility during the entire test. Each of these instruction protocol files produces one results file

562   each that get combined within the AMIDR program. AMIDR is designed to perform comparison

563   between charge and discharge results to confirm accuracy. This does not necessarily have to be

564   unique for AMIDR. While many papers simply report discharge results for GITT, a comparison

565   of charge and discharge results could also be an easy way a lot more confidence to GITT results.

566   Single-rate pulses require three parameters to be selected: voltage limit spacing, the pulse

567   current, and the relaxation time between pulses.

568   Decreasing the voltage limit spacing increases the total number of pulses providing more

569   resolution but also increases test time. There are also hard limits to the voltage limit spacing. The

570   voltage limit spacing must be substantially larger than the instrument's voltage resolution for

571    $Y(\tau) = 1$ to be accurate. Alternatively, the voltage limit spacing must be small enough for the

572   dq/dV of the active material to be consistent throughout the pulse. If two adjacent pulses have a

573   significant difference in dq/dV, then there is likely a large change of dq/dV within each pulse

574   as well. A good rule of thumb is that the dq/dV of a pulse should not differ from a proceeding or

575   succeeding pulse's dq/dV by a factor of 2 or greater. This means that AMIDR struggles with

576   measuring D_c when dq/dV changes rapidly over a small change in V. On a q-V plot these

577   troublesome areas appear as plateaus which are associated with phase changes. One strategy for

578   dealing with these q-V plateaus may be to set a capacity limit in addition to a voltage limit, but

579   this was not attempted for this study.

580   Increasing current decreases the total test time, but current must be set low enough that a

581   complete pulse is achieved by the time the pulse's voltage limit is reached. This is roughly

582   defined as when $\tau > 0.5$, but larger τ values are even more accurate. Considering equation 7

33

583   which describes the lower limit for τ as a result of Q, the maximum current limit can be

584   estimated as $I < 0.5ABdq/dV\Delta V_{tot}D_c r^{-2}$ where ΔV_{tot} can be estimated as the voltage limit

585   spacing. This means that reducing the voltage limit spacing also reduces the maximum current

586   that can be applied increasing test time further. Additionally, current may need to be reduced

587   further for cells with high resistance as this can also cause the voltage limit to be reached

588   prematurely. While this does mean that some parameters need a broad estimate of D_c before

589   testing begins like GITT, it is unlike GITT in that there is a process independent of D_c to detect if

590   the parameters are inadequate after testing.

591   Decreasing relaxation time decreases the test time, but relaxation time must be long

592   enough to achieve "complete" relaxation. Complete relaxation, like complete pulses, is not 100%

593   achievable, but can be approached to a satisfactory level. The amount of time it takes for active

594   material to relax to a uniform concentration is comparable to the amount of time it takes for

595   active material to reach a steady state during a pulse. This is useful because this means that

596   relaxation times that are at least as long as the complete pulses proceeding and succeeding them

597   allow for adequate relaxation. For example, the recommended relaxation time for active material

598   measured with 80 C/80 pulses is > 1 hour as each pulse is expected to last for about 1 hour with

599   some variance due to changing dq/dV. It is recommended to set the relaxation time somewhat

600   longer for active materials with significant change in dq/dV as pulses completed when dq/dV is

601   high will be longer.

602   It is recommended to first determine the desired voltage limit spacing and then select

603   appropriate current and relaxation times dependent on this voltage limit spacing. These

604   parameters can also be adjusted for different ranges of SOC. For instance, it is recommended to

34

605   use smaller voltage limit spacing for ranges of SOC where D_c changes rapidly and smaller

606   current and longer relaxation times for ranges of SOC where D_c is small. In this study, a different

607   set of parameters were selected for active materials at low SOC to compensate for the rapid

608   decrease in D_c typical for layered oxides (see Table S2). For novel materials, AMIDR may have

609   to be run multiple times to tune in each measurement over SOC, but the parameters selected for

610   this study should be adequate for layered oxides. Especially small voltage limit spacing and

611   current are recommended specifically for charging pulses at low SOC. This is because the initial

612   poor D_c at low SOC can cause the first few charging pulses to hit their voltage limits rapidly

613   producing incomplete pulses without enough pulse time for the SOC to change substantially.

614   Eventually a pulse with a voltage limit outside the low SOC range occurs producing a rather long

615   pulse that charges the cell until it is well outside of the low SOC range. Reducing the voltage

616   limit spacing allows for more low SOC pulses to be performed allowing for more capacity to be

617   drawn inside the low SOC range without the voltage limit reaching too far outside. Despite

618   tailored parameter selection for low SOC, the lowest SOC pulses during charge or discharge are

619   generally not complete pulses due to their very poor D_c. If a user can detect that incomplete

620   pulses are being measured during discharge ($\tau > 0.5$), it is recommended to finish that section of

621   the test and start the next charging protocol with a full relaxation step in between. Lastly,

622   changing protocol parameters within the test allows for an additional method of confirmation of

623   results. If results remain continuous when protocol parameters change this informs the user that

624   the protocol parameters are adequate and do not contribute error to the results.

625   It is desired to evenly weigh the pulse datapoints from the start to the end. Regarding

626   Figure 3, this suggests that a logarithmic distribution of Q values would be optimal for sampling

627   with even weighting throughout. Considering $Q = \Delta q_i I^{-1} D_c r^{-2}$ and $\Delta q_i = (dq/dV)\Delta V$, this

35

628   suggests that a logarithmic distribution of Δq_i and therefore ΔV would be ideal, but this is not

629   entirely feasible with most cell testers. Most cell testers do not have an option for designing

630   protocols with logarithmic sampling rates and the voltage resolution of the cell tester might not

631   be accurate enough to properly trigger recording of a datapoint, especially when voltage

632   resolution is being compensated for by averaging of high frequency datapoints. Because Δq_i and

633   Δq only vary by a factor of τ and $\Delta q = I\Delta t$, time sampling is an adequate replacement for

634   voltage sampling. Δq_i and Δq can vary significantly on a logarithmic scale when τ is very small,

635   but the error in τ is also very small when τ is small, so the impact of any "oversampled"

636   datapoints will be negligible and not be consequential to the entire fit. Most cell testers do not

637   have an option for logarithmic time sampling either, but this can be approximated by using a

638   series of steps to approximate a logarithmic distribution. More specifically, a protocol can be

639   designed with a series of seamless CC steps sampling every 0.1 s for 1 s, every 1 s for 9 s, every

640   10 s for 90 s, and so on. This gives a datapoint distribution similar to the tick distribution on a

641   logarithmic plot and an acceptably equal weighting of datapoints across the entire pulse.

642   *Error Management*

643   Not all cells will return accurate results and cells can fail before testing even begins.

644   Because coin cells are not designed with Au wire reference electrodes in mind, the reference

645   electrode can often be the source of cell failure. It is recommended to build three times as many

646   cells as intended to analyse due to the relatively high but manageable rate of cell failure. Firstly,

647   the reference wire may be snipped during the cell crimping step due to the pressure required to

648   seal the cell. Secondly, the insulation surrounding the reference wire may be pierced as well

649   leading to shorts between electrodes. These can either be hard shorts coupling the potentials of

650   two electrodes together, or soft shorts which may not be immediately apparent. Occasionally,

651   delithiation of the reference electrode can be observed when the reference electrode potential

652   strays far away from ~0.31 V vs. Li^+/Li^0, and self-discharge of the cell can be observed when the

653   terminations of rest periods for charge and discharge do not align on a q-V plot (see Figure S6).

654   It is likely that these are due to soft shorts within the coin cell and should be checked before

655   further analysis. Checking for sources of error and outliers is formal part of the analysis process

656   in the AMIDR program.

657   Analysis of quality cells will almost always return some erroneous pulses. There are three

658   ways that erroneous pulses can be detected. Firstly, the pulse data may not be able to fit to the

659   model within the fit parameter bounds. This may be due to a multitude of reasons but most

660   commonly occurs in extreme examples of the other two ways pulses may be detected as

661   erroneous. Secondly, significant changes in dq/dV during a pulse can lead to inaccurate fits as

662   the model expects dq/dV to remain consistent (see Figure S7). This is detected by comparing

663   the dq/dV of pulses with the dq/dV of their adjacent pulses. If there is a difference in dq/dV of

664   a factor of 2 or greater between two adjacent pulses, it is recommended to ignore both pulses.

665   Additionally, it is also recommended to ignore the first and last pulse as their dq/dV cannot be

666   ensured to be steady. Lastly, if a pulse is stopped before diffusive impedance reaches a steady

667   state then that pulse is considered incomplete and should be ignored (see Figure S8). This is

668   recommended to be when the pulse ends with $\tau < 0.5$. This pulse removal process can be done

669   within the AMIDR program and the maximum factor of dq/dV change and the minimum τ can

670   also be adjusted within the AMIDR program. The remaining pulses typically have good fits with

671   low fit error calculated as $\sqrt{\Sigma(\tau_{exp} - \tau_{mod})^2} / (m * \max(\tau_{exp}))$ where τ_{exp} are the relative

37

672   capacities of the experimental dataset, τ_{mod} are the relative capacities of the model sharing the

673   same Q values as τ_{exp}, and m is the total number of τ_{exp} datapoints (see Figure S9 and S10).

674   **Results and Discussion**

675   *Single Cell Example*

676   Figure 9 shows some of the key results returned by AMIDR of a single $LiNi_{0.95}Mn_{0.05}O_2$

677   (NM9505) cell. Most values are plotted with the average voltage of their pulse, but R is plotted

678   with the initial voltage of their pulse as this is primarily where R is realized. It can be

679   immediately observed both in D and R that kinetics get continuously worse at low SOC which

680   aligns with other studies of layered oxides.[11–15] This makes intuitive sense as it is expected that

681   D_c would get worse with additional crowding of ions in the lattice. Kinetics get so sluggish for

682   SOC < 3.6 V that pulses become incomplete suggesting that relaxation times are also incomplete,

683   and the results are erroneous. This results in a lack of agreement between charge and discharge

684   results in D_c, D_t^*, and dq/dV. R appears to still be in good agreement for SOC < 3.6 V because R

685   does not require significant periods of time to develop or relax. There is a mild disagreement

686   between charge and discharge R measurements at SOC 3.65 – 3.85 V which may be due to

687   measurement error but is more likely due to cell R growing during cycling. Results for SOC >

688   4.15 V are erroneous for a different reason. At this SOC, dq/dV increases dramatically which is

689   associated with the H2-H3 phase transition commonly found in high-Ni layered oxides.[16] This

690   dramatic change in dq/dV means that pulses within this region cannot be expected to have a

691   consistent dq/dV and therefore calculation of τ will be inaccurate. The current and relaxation

692   times for SOC 3.6 – 4.15 V can be easily validated as these protocol parameters change at 3.7 V

693   and there are two extra long relaxation times at 3.7 V and 3.95 V between protocol sections, but

694   all results appear continuous at these SOC.

695   D_c and dq/dV are shown to be inversely related to each other for SOC > 3.7 V. This is

696   not coincidental as the greater difference in occupation site potential associated with low dq/dV

697   encourages greater transport from high to low concentration regions. This inverse relationship

698   has interesting implications regarding the calculation of D_t^* using equation 25. D_c and dq/dV

699   cancel each other out leaving behind a relatively consistent D_t^* for SOC > 3.7 V. The derivation

700   of D_t^* given by equation 23 suggests that the average ΔG_A is also mostly consistent within these

701   SOC as ΔG_A is the only term that could conceivably change because of a change of SOC. This

702   derivation could also be used to calculate the average ΔG_A if multiple tests were done at varying

703   T, but this was not accomplished within this study. The cancelling out of this inverse relationship

704   is also present when calculating $R_{D,term}$ using equation 13 leaving a $R_{D,term}$ that is relatively

705   consistent for SOC > 3.7 V despite changing D_c and dq/dV. This makes sense as equation 26

706   shows that ΔG_A is the primary factor determining $R_{D,term}$ and, therefore, the overall long

707   timescale kinetic performance.

708   It is known that a vacancy of the target occupation site is necessary for site hopping

709   transportation to occur and this is accounted for in deriving D_t^*. However, it has also been shown

710   that an additional, adjacent vacancy allows for a transport pathway through an intermediate

711   tetrahedral site reducing ΔG_A. This is known as divacancy hopping and is the dominant mode of

712   transport when available.[15] Divacancies become uncommon when the layered oxide is more

713   saturated at low SOC and therefore the average ΔG_A increases with further saturation in

714   agreement with the downward trend of D_t^* for SOC < 3.7 V. Much more recently, it has also

715   been shown that even if both adjacent occupation sites are occupied by lithium atoms, low ΔG_A

716   site hops with similar ΔG_A to that of divacancy hops can occur if the doubly-adjacent occupation

717   sites are vacant.[17] This particular study is still undergoing peer review, but gives a better

39

718   explanation for why D_t^* is constant at SOC > 3.7 V where divacancies may still be uncommon,

719   but doubly-adjacent occupation sites are still commonly vacant.

720   The benefits of using AMIDR to determine R are shown as well. A common, traditional

721   method to measure R is to calculate it as $R = \Delta V_1/I$, where ΔV_1 is the initial change in voltage

722   between the first two datapoints of the pulse. However, the exact value of ΔV_1 is dependent on

723   the sampling rate selected by the user or limited by the cell tester. If the sampling rate is too fast

724   such as measuring once every 0.05 s, R may be underestimated as the total η_R may not be fully

725   realized due to delay from capacitive effects. If the sampling rate is too slow such as measuring

726   once every 5 s, R may be overestimated as a significant portion of η_D will be measured with η_R.

727   This suggests that you might have a window of accuracy with a sampling rate such as once every

728   0.5 s, but this just includes both errors. It can be seen that R measured with the ΔV_1 after 0.5 s is

729   overestimated at high SOC and underestimated at low SOC. The minimum time it takes for η_R to

730   be realized is dependent on the total amount of R, so there is no optimal sampling rate for

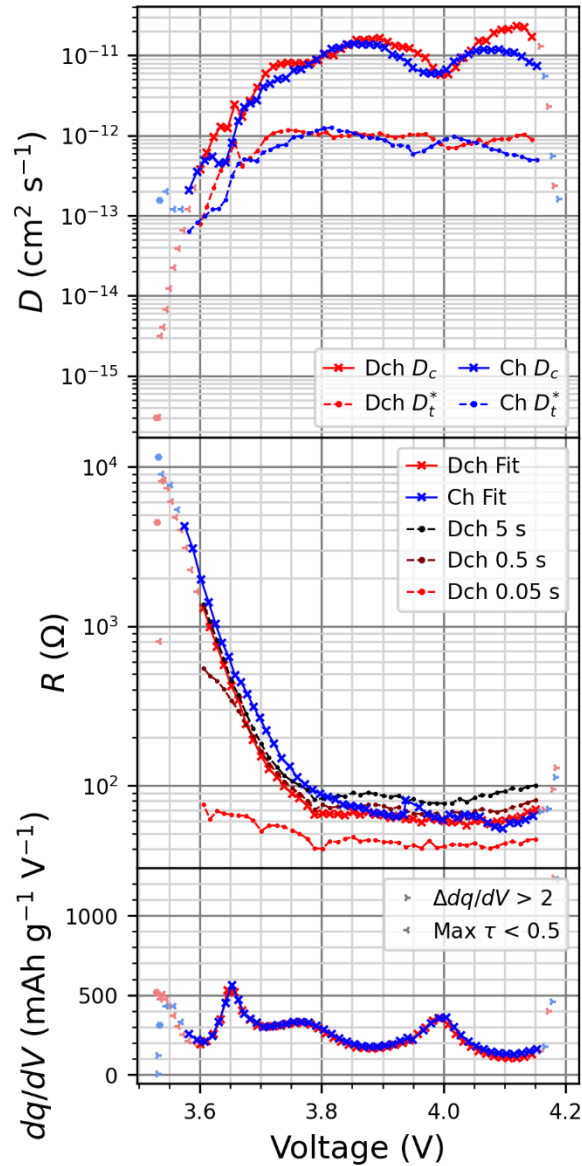731   accurately measuring all possible values of R.

Figure 9: AMIDR results of a single NM9505 cell at 30 °C. Incomplete pulses and poor kinetics are common at low SOC and large dq/dV changes are common at the H2-H3 phase transition > 4.15 V. Chemical diffusivity, D_c, varies inversely with dq/dV leaving a relatively flat free-path tracer diffusivity, D_t^*. Resistance, R, measured from initial voltage changes is either underestimated or overestimated compared to fit R for all sampling rates. D_t^* and initial voltage change R results from erroneous pulses are not shown for clarity.

Charge/Discharge Disagreement

While charge and discharge results generally align, there is a measurable difference between the two that curiously revolves around dq/dV peaks and valleys. Figure 10a shows binned and averaged data from multiple cells using a beta protocol from early in AMIDR

41

743   development. It's apparent that the calculated D_c and D_t^* values are higher when dq/dV is

744   decreasing during a pulse and vice versa. This suggests that change in dq/dV produced error in

745   the calculated D values. One explanation is that decreasing dq/dV gives the impression that the

746   η_D in the middle of a pulse is smaller than it's expected to be, overestimating D_c in the fitting.

747   The opposite would occur for increasing dq/dV and the error would be minimized for pulses

748   upon dq/dV peaks and valleys as the dq/dV change is also minimized. Figure 10b shows data

749   from a newer, high resolution protocol developed in response to this charge/discharge

750   disagreement with voltage limit spacing half the size of the beta protocol. Charge/discharge

751   disagreement is still apparent with the high resolution protocol but appears to be marginally

752   improved.

753   An issue making comparison of these two datasets difficult is that the beta protocol cells

754   were coated on a rougher than ideal surface which encouraged active material agglomeration.

755   Unfortunately, these cells were built early in development of AMIDR before the issue of a rough

756   coating surface was realized. This agglomeration caused groups of particles to act as larger

757   particles giving the impression of smaller D_c with higher variance. The agglomeration produced

758   consistently higher fit errors, even for pulses upon dq/dV peaks and valleys.
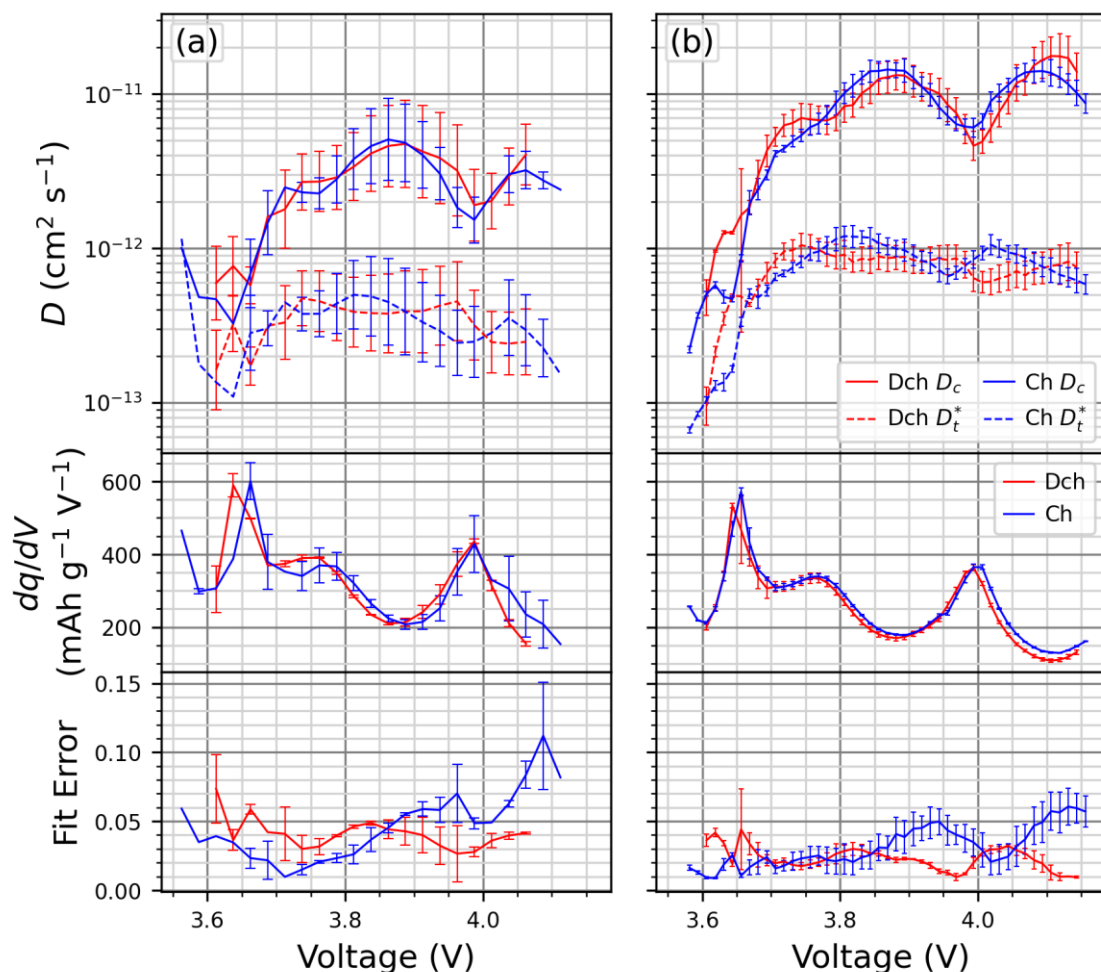
Figure 10: Comparison of NM9505 cells at 30 °C tested with (a) an early beta protocol and (b) a high resolution protocol. Additionally, the cells made for the beta protocol were coated on a rough surface and had issues with particle agglomeration. Cell data was binned into voltage ranges and averaged. Both protocols generated charge/discharge disagreement in diffusivity, D, revolving around dq/dV peaks and valleys. The high resolution protocol shows larger D values with less charge/discharge disagreement, variance, and fit error.

Counter Electrode Impact

Because charge and discharge data have opposite errors, they can be binned and averaged together to return results agnostic of current direction. Figure 11 shows averaged data from NM9505 cells with both the impedance against the reference electrode and impedance against the lithium metal anode analyzed by AMIDR. These cells had minimal cathode mass loading to amplify the cathode impedance and to eliminate electrolyte pore impedance. However, even with amplified cathode impedance, the lithium metal anode still produced enough impedance to skew

43

773 results measurably for SOC > 3.7 V where cathode impedance is small. If high accuracy is not

774 desired, it may be acceptable to simply test 2-electrode coin cells as they are far easier to make.

775 However, if 2-electrode coin cells are tested, it is strongly recommended to compare their results

776 to the impedance of lithium metal symmetrical cells to ensure that it is not simply lithium metal

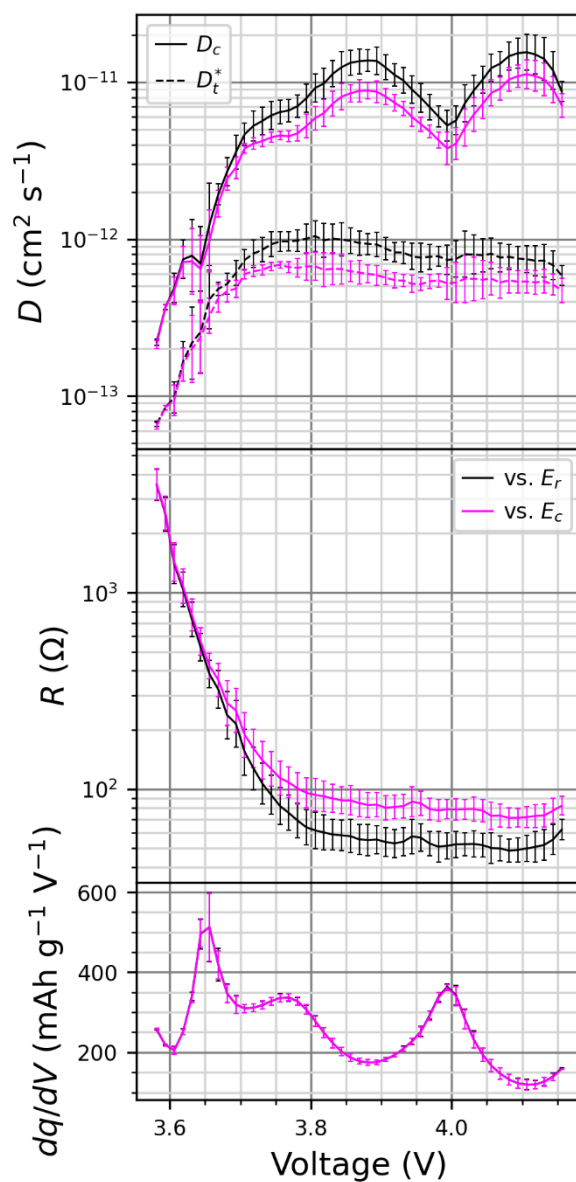777 impedance that is being measured.

778
779   Figure 11: Comparison of NM9505 cells at 30 °C analyzed with impedance against the reference
780   electrode potential, E_r, and impedance against the counter electrode potential, E_c. Even with minimal

781   cathode mass loading to amplify cathode impedance, impedance from a lithium metal anode can obscure
782   diffusivity, D, measurements.

783   *Material Comparisons*

784   Figure 12 shows the difference in kinetics of three different types of commercial layered

785   oxide active materials. It can be immediately seen that $LiNi_{0.8}Mn_{0.1}Co_{0.1}O_2$ (NMC811) and

786   NM9505 have very similar kinetic performance as high-Ni layered oxides with a similar

787   proportion of Ni in the Li layer, Ni_{Li}, determined with XRD (see Figure S4 and Table S4). D_c at

788   the 4.0 V q-V plateau unique to NM9505 is somewhat worse than NMC811, but this q-V plateau

789   has similar overall kinetic performance due to having a similar D_t^* and therefore similar $R_{D,term}$.

790    $LiNi_{0.6}Mn_{0.4}O_2$ (NMC640), however, shows much worse kinetic performance at most SOC. This

791   is because the NMC640 has higher Ni_{Li} which prevents divacancy hops at adjacent sites.

792   However, at low SOC where the active material has high Li saturation, NMC640 shows similar

793   kinetic performance to the other materials as divacancies are uncommon for all materials at this

794   SOC.

795   The three commercial materials also have very similar maximum ρ_c as a function of

796   voltage. It's important to recognize this measurement as a maximum value because a certain

797   amount of R in the cell is not sourced from the active material surface. However, R_i is the only

798   source of R that could conceivably change with SOC, so it's fair to regard the larger values of ρ_c

799   as effectively entirely due to R_i as other sources of R would be negligible. It's hard to determine

800   whether R_i is primarily due to a single charge transfer reaction or a thin, low D_c surface layer as

801   they both generate R_i independent of the currents applied. If it is a single charge transfer reaction

802   between the electrolyte and the active material, then it would be expected to follow the Butler-

803   Volmer equation. However, the relationship between current density, $j = I/S$, and η in the

804   Bulter-Volmer equation is linear for $\eta < 25$ mV and no pulse had $\eta > 25$ mV as the voltage limit

45

805   spacing was set at 25 mV or less. The expected charge transfer resistance, R_{ct}, would therefore

806   follow Ohm's law and be consistent across varying I. R_i may also be due to a negligible charge

807   transfer reaction and a thin, low D_c surface layer. Commercial active material is often engineered

808   with surface treatments to extend cycle life and a reconstructed rock salt surface layer is often

809   observed for layered oxides.[18] A thin surface layer can be modeled as a thin, low D_c phase

810   effectively producing an R_i that also follows Ohm's law on a reasonably short timescale (see

811   Proof 3). It is possible that the observed increase in R_i during the charge pulses after the

812   discharge pulses is due to a thickening of this surface layer. However, it's also possible that the

813   observed increase in R_i may also be due to a decrease in active material surface area accessible

814   to charge transfer due to the growth of an impenetrable surface layer. Regardless, it's clear that

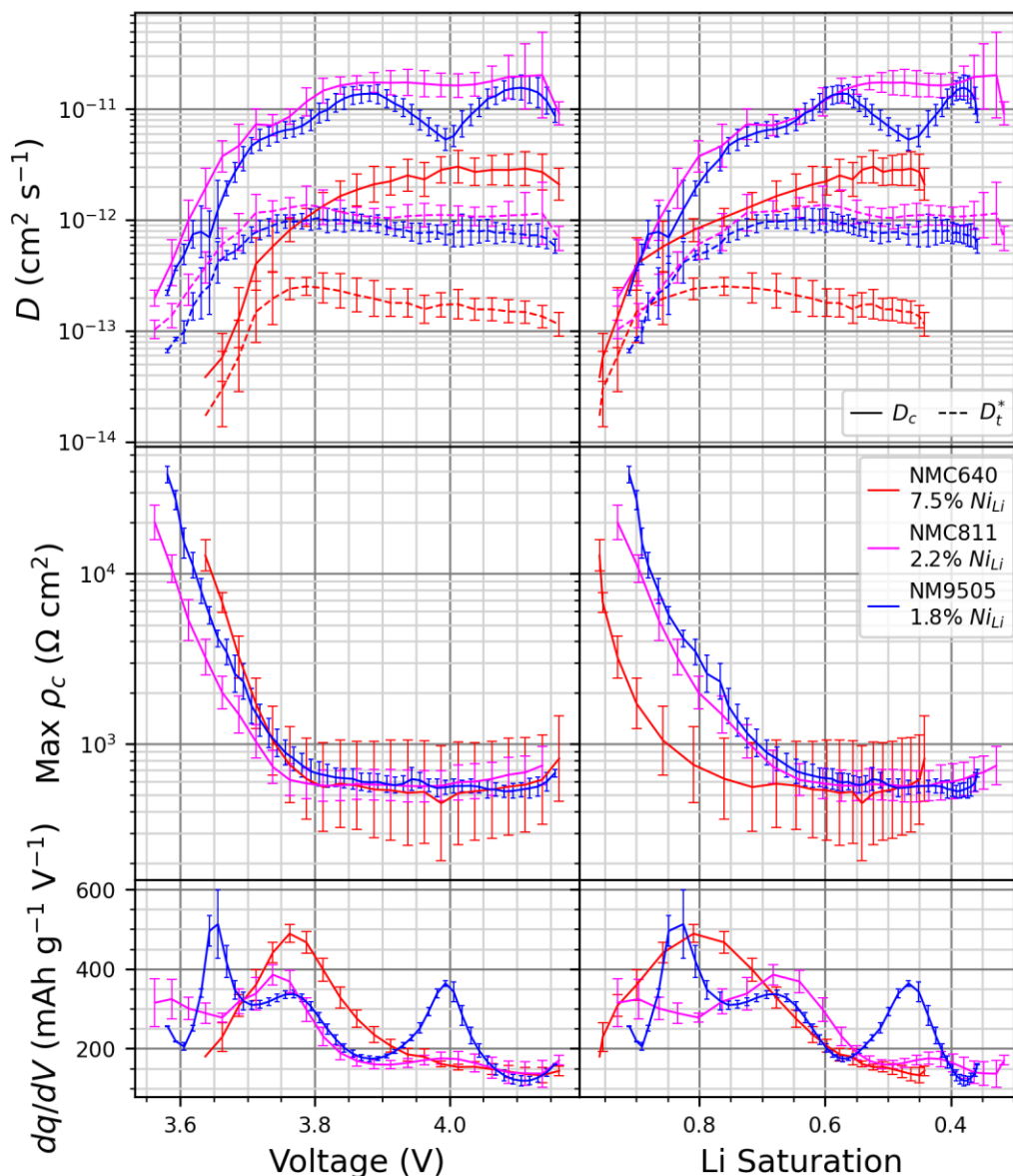815 R_i is heavily dependent on SOC in a manner similar to D_c.

Figure 12: Comparison of commercial layered oxide materials at 30 °C. NMC811 and NM9505 show similar kinetics with similar Ni in Li layer, Ni_{Li}, measured with XRD. NMC640 has additional Ni_{Li} and worse kinetics.

Conclusion

AMIDR is an improved method for measuring D_c due to a series of important design decisions that all must be considered to achieve accuracy. Notably, test cells are designed to amplify active material impedance and ignore impedance from the opposing electrode, the cell testing protocol and analysis are designed to measure complete pulses which reach a steady state,

47

825   the analysis program is designed to calculate both cell R and D_c simultaneously by fitting to a

826   complete pulse model, and extra care is taken to detect and remove erroneous outliers and

827   achieve effective charge/discharge agreement. With careful application of this method, insight

828   into the mechanistic construction of D_c and R_i is revealed. In addition, three different layered

829   oxide materials were analyzed, and their results compared giving further evidence that layered

830   oxide D_c is heavily dependent on Ni_{Li}, but not necessarily at low SOC.

831   **List of Symbols**

832   a distance between two occupation sites (cm)

833   A geometric constant (1 for a planar sheet, 2 for a cylinder, 3 for a sphere)

834   α_i series of geometric constants defined by equations

835   B geometric constant (3 for a planar sheet, 4 for a cylinder, 5 for a sphere)

836   c ion concentration (mol cm^{-3})

837   c_s surface c (mol cm^{-3})

838   c_{sat} c of a completely saturated active material (mol cm^{-3})

839   Δc_s change in c_s after a certain Δt (mol cm^{-3})

840        $\Delta c_{s,loss}$ deviation in c_s from impedance-free scenario (mol cm^{-3})

841   Δc_{tot} change in c if n_{tot} moles are evenly transported (mol cm^{-3})

842   C dimensionality constant

843   dE/dc relationship between c and E at any given SOC

844   dq/dV relationship between V and q at any given SOC

845   D_c chemical diffusivity (cm^2 s^{-1})

846   D_t tracer diffusivity (cm^2 s^{-1})

847   D_t^* free-path tracer diffusivity (cm^2 s^{-1})

848   E electrode potential (V)

849   E_c counter E (V)

850   E_w working E (V)

851   F Faraday's constant (C mol^{-1})

852   ΔG_A occupation site hop activation energy (J)

48

853	I	applied current (A)
854	J	ionic flux (mol s^{-1} cm^{-2})
855	J_1	Bessel function of the first kind of order 1
856	k_B	Boltzmann constant (J K^{-1})
857	m	active material mass (g)
858	n	moles of ions transported after a certain Δt (mol)
859	n_{tot}	moles of ions desired to be transported (mol)
860	N_A	Avogadro constant (mol^{-1})
861	P	relative resistance
862	q	capacity (C)
863	q_e	elementary charge (C)
864	q_{sat}	theoretical q of a fully saturated active material (C)
865	Δq	change in q after a certain Δt (C)
866	Δq_c	cumulative change in q of a series of pulses (C)
867	Δq_i	ideal, impedance-free change in q corresponding to ΔV (C)
868	Δq_{tot}	change in q if n_{tot} moles are transported (C)
869	Δq_0	change in q after a pulse and relaxation (C)
870	Q	relative D_c
871	r	diffusion length or radius (cm)
872	$\bar{r}$	capacity-weighted geometric mean of r (cm)
873	$\bar{r}_e$	average r for modeling end of pulse (cm)
874	$\bar{r}_s$	average r for modeling start of pulse (cm)
875	R	resistance (Ω)
876	$R_{D,term}$	terminal diffusive R (Ω)
877	R_i	interface R (Ω)
878	R_{ohm}	combined electrical contact R and ionic electrolyte R (Ω)
879	S	electrode surface area (cm^2)
880	t	time (s)
881	Δt	pulse time (s)
882	T	temperature (K)

883   V cell voltage (V)

884   ΔV change in V after a certain Δt (V)

885   ΔV_i ideal ΔV in an impedance-free scenario (V)

886   ΔV_{tot} ΔV if n_{tot} moles are transported and active material allowed to relax (V)

887   ΔV_0 change in V after a pulse and relaxation (V)

888   ΔV_1 initial ΔV at start of pulse (V)

889        $\tilde{V}$ electrode volume (cm^3)

890   X_s relative Δc_s

891        $X_{s,loss}$ deviation in X_s from impedance-free scenario

892        $X_{s,ideal}$ ideal X_s under an impedance-free scenario

893   Y relative ΔV

894   z ion charge number

895   γ activity coefficient

896   η overpotential (V)

897   η_D diffusion η (V)

898   η_R resistance η (V)

899   μ chemical potential (J mol^{-1})

900   μ_0 intrinsic chemical potential (J mol^{-1})

901   ν vibrational frequency (s^{-1})

902   ρ_c interface contact resistivity (Ω cm^2)

903   ρ_d active material density (g cm^{-3})

904   τ relative Δq

Acknowledgement

909

References

1. S. Atlung, K. West, and T. Jacobsen, *J. Electrochem. Soc.*, **126**, 1311–1321 (1979).

2. C. Deng and W. Lu, *Journal of Power Sources*, **473**, 228613 (2020).

3. B. Choudhury, A. Jangale, and B. Suthar, *J. Electrochem. Soc.*, **170**, 070519 (2023).

4. H. H. Berger, *J. Electrochem. Soc.*, **119**, 507 (1972).

5. C. Liu, Z. G. Neale, and G. Cao, *Materials Today*, **19**, 109–123 (2016).

6. O. J. Kleppa, *Annu. Rev. Phys. Chem.*, **6**, 119–140 (1955).

7. Y. Fujihara and T. Kobayashi, *J. Electrochem. Soc.*, **169**, 080509 (2022).

8. M. Doyle, J. Newman, and J. Reimers, *Journal of Power Sources*, **52**, 211–216 (1994).

9. S. Solchenbach, D. Pritzl, E. J. Y. Kong, J. Landesfeind, and H. A. Gasteiger, *J. Electrochem. Soc.*, **163**, A2265–A2272 (2016).

10. Y.-C. Chien, D. Brandell, and M. J. Lacey, *Chem. Commun.*, **58**, 705–708 (2022).

11. A. Liu, N. Phattharasupakun, M. M. E. Cormier, E. Zsoldos, N. Zhang, E. Lyle, P. Arab, M. Sawangphruk, and J. R. Dahn, *J. Electrochem. Soc.*, **168**, 070503 (2021).

12. E. S. Zsoldos, M. M. E. Cormier, M. Ball, D. Rathore, and J. R. Dahn, *J. Electrochem. Soc.*, **170**, 070502 (2023).

13. E. Zsoldos, M. M. E. Cormier, N. Phattharasupakun, A. Liu, and J. R. Dahn, *J. Electrochem. Soc.*, **170**, 040511 (2023).

14. Y.-C. Chien, H. Liu, A. S. Menon, W. R. Brant, D. Brandell, and M. J. Lacey, *Nat Commun*, **14**, 2289 (2023).

15. A. Van Der Ven and G. Ceder, *Journal of Power Sources*, **97–98**, 529–531 (2001).

16. J. Chen, H. Yang, T. Li, C. Liu, H. Tong, J. Chen, Z. Liu, L. Xia, Z. Chen, J. Duan, and L. Li, *Front. Chem.*, **7**, 500 (2019).

17. P. Xiao, N. Zhang, H. S. Perez, and M. Park, (2023) https://arxiv.org/abs/2311.06140.

18. F. Lin, I. M. Markus, D. Nordlund, T.-C. Weng, M. D. Asta, H. L. Xin, and M. M. Doeff, *Nat Commun*, **5**, 3529 (2014).